diseases favor the H-latch, according to MD simulations. These observations suggest that the H-latch is not only involved in the toxicity of anti-PrP antibodies, but also in the pathogenesis of prion diseases.

Spongiform change, that is endolysosomal hypertrophy through UPR activation and subsequent PIKfyve depletion, is shared in both prion and POM1 toxicity[21]. Multiple toxic cascades are activated in prion infections and in cells treated with POM1 (ref. [8]). Cells that stably express PrP^{2cys} are not affected by UPR in the current experimental paradigm, suggesting that either the protein dosage is insufficient to observe UPR or its toxicity is independent of PIKfyve depletion. Besides neuronal loss, which is shared among prion, POM1 and PrP^{2cys} toxicity, it will be interesting to investigate the overlap of toxic cascades between the different prion disease models, which could provide important knowledge of early disease-associated changes.

The above findings hold promise for therapeutic interventions. First, the POM1 binding region includes a well-defined pocket created by the α1–α3 helix of PrP^{C}, which may be targeted by therapeutic compounds including antibodies, small molecules, cyclic peptides or aptamers. Second, ^{hc}Y104A halted progression of prion toxicity even when it was already conspicuous, whereas the anti-FT antibody POM2 exerted neuroprotection only when applied directly after prion inoculation[11]. This suggests that ^{hc}Y104A halts prion toxicity upstream of FT engagement[8,11]. Thirdly, tga20 COCS (which are much more responsive to toxic pomologs than wild-type COCS, and can therefore be regarded as a sensitive sentinel system) tolerated prolonged application of ^{hc}Y104A at concentrations around 150 × K_D. Finally, intracerebrally injected ^{hc}Y104A was innocuous, and AAV-transduced ^{hc}Y104A extended the lifespan of prion-infected mice, despite elevated PrP^{Sc} levels, suggesting that it acts downstream of PrP^{Sc} replication, possibly by blocking a PrP^{Sc}-PrP^{C} interaction at the POM1 epitope. These findings suggest that blockade of the POM1 epitope by agents that do not induce the H-latch has good in vivo tolerability. In view of the reports that PrP^{C} may mediate the toxicity of disparate amyloids[22], the relevance of the above findings may extend to proteotoxic diseases beyond spongiform encephalopathies.

Online content

Any methods, additional references, Nature Research reporting summaries, source data, extended data, supplementary information, acknowledgements, peer review information; details of author contributions and competing interests; and statements of data and code availability are available at https://doi.org/10.1038/s41594-022-00814-7.

Received: 1 December 2021; Accepted: 6 July 2022;
Published online: 10 August 2022

References

1. Brandner, S. et al. Normal host prion protein necessary for scrapie-induced neurotoxicity. *Nature* **379**, 339–343 (1996).
2. Lakkaraju, A. K. K. et al. Loss of PIKfyve drives the spongiform degeneration in prion diseases. *EMBO Mol. Med.* **13**, e14714 (2021).
3. McNally, K. L., Ward, A. E. & Priola, S. A. Cells expressing anchorless prion protein are resistant to scrapie infection. *J. Virol.* **83**, 4469–4475 (2009).
4. Wulf, M. A., Senatore, A. & Aguzzi, A. The biological function of the cellular prion protein: an update. *BMC Biol.* **15**, 34 (2017).
5. Bueler, H. et al. Mice devoid of PrP are resistant to scrapie. *Cell* **73**, 1339–1347 (1993).
6. Heppner, F. L. et al. Prevention of scrapie pathogenesis by transgenic expression of anti-prion protein antibodies. *Science* **294**, 178–182 (2001).
7. Sonati, T. et al. The toxicity of antiprion antibodies is mediated by the flexible tail of the prion protein. *Nature* **501**, 102–106 (2013).
8. Herrmann, U. S. et al. Prion infections and anti-PrP antibodies trigger converging neurotoxic pathways. *PLoS Pathog.* **11**, e1004662 (2015).
9. Reimann, R. R. et al. Differential toxicity of antibodies to the prion protein. *PLoS Pathog.* **12**, e1005401 (2016).
10. Frontzek, K. et al. Neurotoxic antibodies against the prion protein do not trigger prion replication. *PLoS ONE* **11**, e0163601 (2016).
11. Bardelli, M. et al. A bispecific immunotweezer prevents soluble PrP oligomers and abolishes prion toxicity. *PLoS Pathog.* **14**, e1007335 (2018).
12. Baral, P. K. et al. Structural studies on the folded domain of the human prion protein bound to the Fab fragment of the antibody POM1. *Acta Crystallogr. Sect. D Biol. Crystallogr.* **68**, 1501–1512 (2012).
13. Mahal, S. P. et al. Prion strain discrimination in cell culture: the cell panel assay. *Proc. Natl Acad. Sci. USA* **104**, 20908–20913 (2007).
14. Falsig, J. et al. A versatile prion replication assay in organotypic brain slices. *Nat. Neurosci.* **11**, 109–117 (2008).
15. Nuvolone, M. et al. Strictly co-isogenic C57BL/6J-*Prnp*$^{-/-}$ mice: a rigorous resource for prion science. *J. Exp. Med.* **213**, 313–327 (2016).
16. Fischer, M. et al. Prion protein (PrP) with amino-proximal deletions restoring susceptibility of PrP knockout mice to scrapie. *EMBO J.* **15**, 1255–1264 (1996).
17. Perrier, V. et al. Anti-PrP antibodies block PrPSc replication in prion-infected cell cultures by accelerating PrPC degradation. *J. Neurochem.* **89**, 454–463 (2004).
18. White, A. R. et al. Monoclonal antibodies inhibit prion replication and delay the development of prion disease. *Nature* **422**, 80–83 (2003).
19. Simonelli, L. et al. Mapping antibody epitopes by solution NMR spectroscopy: practical considerations. *Methods Mol. Biol.* **1785**, 29–51 (2018).
20. Wang, J. et al. A human bi-specific antibody against Zika virus with high therapeutic potential. *Cell* **171**, 229–241(2017).
21. Lakkaraju, A. K. et al. Loss of PIKfyve drives the spongiform degeneration in prion diseases. *EMBO Mol. Med.* **13**, e14714 (2021).
22. Brody, A. H. & Strittmatter, S. M. Synaptotoxic signaling by amyloid beta oligomers in Alzheimer's disease through prion protein and mGluR5. *Adv. Pharm.* **82**, 293–323 (2018).

Methods

Adeno-associated virus production and in vivo transduction. Single-stranded adeno-associated virus (ssAAV) vector backbones with AAV2 inverted terminal repeats (ITRs) were kindly provided by B. Schneider (EPFL). Herein, expression of the monomeric NeonGreen fluorophore was driven by the human Synapsin I (hSynI) promoter. A P2A sequence (GSGATNFSLLKQAGDVEENPGP) was introduced between mNG and PrP^{C} for bi-cistronic expression. For $mPrP^{R207A}$ and $mPrP^{2cys}$ expression, a synthetic gene block (gBlock, IDT, full sequence is given in the Supplementary Information) was cloned between the BsrGI and HindIII site of the vector replacing the wild-type PrP^{C} sequence. Recombination of plasmids was tested using SmaI digestion prior to virus production. The viral vectors and viral vector plasmids were produced as hybrid AAV2/6 (AAV6 capsid with AAV2 ITRs) by the Viral Vector Facility (VVF) of the Neuroscience Center Zurich. The identity of the packaged genomes was confirmed by Sanger DNA-sequencing (identity check). Quantification of mNG-positive cells from confocal images was done using the Spots function in Imaris (Bitplane).

Neurotropic AAV variants for scFv antibody expression were constructed from a synthetic gene fragment, NheI-IL2-scFv-Myc-EcoRV (produced by Genscript Biotech), which contained ^{hc}Y104A sequences preceded by the signal peptide from interleukin-2 (IL-2)[23]. NheI and EcoRV restriction-enzyme digestion was performed on NheI-IL2-scFv-Myc-EcoRV synthetic gene fragments, which were then inserted into a ssAAV vector backbone. ScFv expression was under the control of the strong, ubiquitously active CAG promoter. A WPRE (woodchuck hepatitis virus post-transcriptional regulatory element) sequence was also included, downstream of the transgene, to enhance transgene expression. Production, quality control and determination of vector titer was performed by ViGene Biosciences). Rep2 and CapPHP.B plasmids were provided under a Material Transfer Agreement (MTA). Further details about packaging and purification strategies can be found on the company's website (http://www.vigenebio.com).

Allen Mouse Brain Atlas data. Images from in situ hybridization for calbindin 1 and synapsin 1 expression were taken from the Allen Mouse Brain Atlas (www.brain-map.org). The first dataset retrieved by the R package allenbrain (https://github.com/oganm/allenBrain) with the closest atlas image to the center of the region (regionID = 512, settings: planeOfSection = 'coronal', probeOrientation = 'antisense') was downloaded (dataset ID nos. for calb1 = 71717640, syn1 = 227540).

Animals and in vivo experiments. We conducted all animal experiments in strict accordance with the Swiss Animal Protection law and dispositions of the Swiss Federal Office of Food Safety and Animal Welfare (BLV). The Animal Welfare Committee of the Canton of Zurich approved all animal protocols and experiments performed in this study (animal permits 123, ZH90/2013, ZH120/16, ZH139/16). Genetically modified mice from the following genotypes were used in this study: Zurich I mice homozygous for disrupted *Prnp* genes ($Prnp^{o/o}$, denoted as $Prnp^{ZH1/ZH1}$)[5], Zurich III $Prnp^{o/o}$ (denoted as $Prnp^{ZH3/ZH3}$)[15] and tga20 (ref. [16]).

For in vivo transduction with the neurotropic AAV-PHP.B construct, mice received a total volume of 100 µL (1×10^{11} total vector genomes) by intravenous injection into the tail vein. Fourteen days after AAV transduction, the left hemispheres of Tga20 mice were innoculated with 30 µL of 0.1% RML6 brain homogenate, corresponding to 3×10^{5} median lethal dose (LD_{50}; 3.6 µg of total brain homogenate). Brain homogenates were prepared in 0.32 M sucrose in PBS at a concentration of 10% (wt/vol). Protein analysis of mouse brains is described below.

After fixation with 4% paraformaldehyde for 1 week, tissues were treated with concentrated formic acid for 60 minutes, fixed again in formalin and eventually embedded in paraffin. HE staining and SAF84 immunohistochemistry were performed as previously described[24]. For immunohistochemical detection of Myc-tag, tissue was deparaffinized and incubated in citrate buffer (pH 6.0) in a domestic microwave for 20 minutes. Unspecific reactivity was blocked using blocking buffer (10% goat serum, 1% bovine serum albumin, 0.1% Triton X-100 in PBS) for 1 hour at room temperature. Primary rabbit anti-Myc-tag antibody (1:500, ab9106, Abcam, overnight at 4 °C) was detected with Alexa Fluor 594 rabbit anti-goat (IgG) secondary antibody (1:1,000, 1 hour at room temperature), diluted in staining buffer (1% bovine serum albumin, 0.1% Triton X-100 in PBS). Tissue was counterstained with DAPI (5 µg/ml, 15 minutes at room temperature).

Cell lines. CAD5 is a subclone of the central nervous system catecholaminergic cell line CAD showing particular susceptibility to prion infection[10]. Generation of the CAD5 $Prnp^{-/-}$ clone no. C12 was described before, as was overexpression of murine, full-length PrP^{C} in CAD5 $Prnp^{-/-}$ by cloning the open reading frame of *Prnp* into the pcDNA3.1(+) vector, *Prnp* expression was driven by a constitutively expressed cytomegalovirus promoter (yielding pcDNA3.1(+)-*Prnp*) as described earlier[13]. For stable expression of $mPrP^{2cys}$, pcDNA3.1(+)-*Prnp* vector was modified using Quikchange II Site-Directed Mutagenesis Kit (Agilent), according to the manufacturer's guidelines. We first introduced a mutation leading to p.R207C (primers (5′→3′): mutagenesis forward: GTG-AAG-ATG-ATG-GAG-TGC-GTG-GTG-GAG-CAG-A, reverse: TCT-GCT-CCA-CCA-CGC-ACT-CCA-TCA-TCT-TCA-C) which was then followed by the p.I138C mutation (mutagenesis forward: AGT-CGT-TGC-CAA-AAT-GGC-ACA-TGG-GCC-TGC-TCA-TGG, reverse: CCA-TGA-GCA-GGC-CCA-TGT-GCC-ATT-TTG-GCA-ACG-ACT). For stable expression of $mPrP^{R207A}$, pcDNA3.1(+)-*Prnp* was mutated correspondingly (mutagenesis forward: TGT-GAA-GAT-GAT-GGA-GGC-CGT-GGT-GGA-GCA-GAT-G, reverse: TCT-GCT-CCA-CCA-CGC-ACT-CCA-TCA-TCT-TCA-C).

Cell vacuolation assay. Mouse hypothalamic Gt1 neuronal cells were grown in Dulbecco's Modified Eagle Medium (DMEM) in the presence of 10% fetal bovine serum (FBS), 1% penicillin–streptomycin and 1% glutamax (all obtained from Invitrogen). For prion infection of the cells, Gt1 cells grown in DMEM were incubated with either Rocky mountain laboratory strain of prion (RML6) prions (0.1%) or non-infectious brain homogenate (NBH; 0.1%) for 3 days in 1 well of a 6-well plate. This was followed by splitting the cells at a 1:3 ratio every 3 days for at least 10 passages. The presence of infectivity in the cells was monitored by the presence of PK-resistant PrP, as described below. At 70 days postinfection (dpi), the cells started developing vacuoles, which were visualized by phase-contrast microscopy. Antibody treatment with ^{hc}Y104A was administered on 70–75 dpi at a concentration of 180 nM.

Cerebellar organotypic slice cultures. Mice from C57BL/6, tga20, $Prnp^{ZH1/ZH1}$ and $Prnp^{ZH3/ZH3}$ strains were used for preparation of COCS, as described[14]. Herein, 350-µm-thick COCS were prepared from 9- to 12-day-old pups. Free-floating sections of COCS were infected with 100 µg prions per 10 slices of RML6 (passage 6 of the Rocky Mountain Laboratory strain mouse-adapted scrapie prions) or 22L (mouse-adapted scrapie prions) brain homogenate from terminally sick, prion-infected mice. Brain homogenate from CD1-inoculated mice was used as non-infectious brain homogenate (NBH). Sections were incubated with brain homogenates diluted in physiological Grey's Balanced Salt Solution for 1 hour at 4 °C and washed, and 5–10 slices were placed on a 6-well PTFE membrane insert. Analogously, for AAV experiments, COCS were incubated with AAV at a final concentration of 5.2×10^{10} total vector genomes diluted in physiological Grey's Balanced Salt Solution for 1 hour at 4 °C, then washed and placed on PTFE membrane inserts. Antibody treatments were given thrice weekly, e.g. with every medium change. In naive slices, antibody treatments were initiated after a recovery period of 10–14 days.

For testing of innocuity of pomologs (Fig. 2c, Supplementary Fig. 7c and Supplementary Fig. 10), POM1 and pomolog antibodies were added at 400 nM for 14 days. Supplementary Figures 7c and 10 represent aggregated data from multiple experiments with COCS from mice of identical genotype and age; compounds were administered at identical timepoints and dosage. When added to RML-infected tga20 COCS (Fig. 2d and Supplementary Fig. 7d), ^{hc}Y57A was added from 20 to 45 dpi, ^{hc}Y104A was added from 21 to 45 dpi and both antibodies were given at 400 nM. Antibody treatment with ^{hc}Y57A and ^{hc}Y104A of RML-infected tga20 COCS used for determination of PrP^{Sc} by western blot, see detailed protocol below, was initiated and stopped at 21 dpi and 45 dpi, respectively. ^{hc}D55A was added to RML-infected tga20 COCS at either 1 (800 nM, Supplementary Fig. 12d) or 21 (400 nM, Fig. 2d and Supplementary Fig. 7d) dpi. When added to C57BL/6 COCS (Fig. 2e and Supplementary Fig. 7e), hc^{Y104A} was added from 1 dpi at 400 nM until 45 dpi. In 22L-inoculated COCS, ^{hc}Y104A was administered at 21 dpi, and slices were collected at 44 dpi. Phage-derived Fabs were added to RML-infected COCS (Fig. 4b–g) from 1 dpi until 45 dpi at 550 nM.

ELISA. PrP^{C} levels were measured by ELISA using monoclonal anti-PrP^{C} antibody pairs POM19/POM3 or POM3/POM2 (all as holo-antibodies), as described previously[25]. First, 384-well SpectraPlates (Perkin Elmer) were coated with 400 ng mL^{-1} POM19 (POM3) in PBS at 4 °C overnight. Plates were washed 3 times in 0.1% PBS-Tween 20 (PBS-T) and blocked with 80 µL 5% skim milk in 0.1% PBS-T per well for 1.5 hours at room temperature. Blocking buffer was discarded, and samples and controls were dissolved in 1% skim milk in 0.1% PBS-T for 1 hour at 37 °C. Twofold dilutions of $rmPrP_{23-231}$, starting at a dilution of 100 ng/mL in 1% skim milk in 0.1% PBS-T, were used as a calibration curve. Biotinylated POM3 (POM2) was used to detect PrP^{C} (200 ng/mL in 1% skim milk in 0.1% PBS-T), and biotinylated antibodies were detected with streptavidin-HRP (1:1,000 in 1% skim milk in 0.1% PBS-T, BD Biosciences). Chromogenic reaction and reading of plates were performed as described in ref. [25]. Unknown PrP^{C} concentrations were interpolated from the linear range of the calibration curve using linear regression (GraphPad Prism, GraphPad Software).

ELISA screening of phage display. Single colonies were picked and cultured in a 384-well plate (Nunc) in 2YT, ampicillin and 1% glucose medium overnight at 37 °C, 80% humidity, 500 r.p.m. These precultures were used to prepare glycerol stock master plates. Expression plates were prepared from the master plates by inoculating corresponding wells with 2YT, carbenicillin and 0.1% glucose medium, followed by induction with 1 mM IPTG. After 4 hours at 37 °C, 80% humidity, cultures were lysed for 1.5 hours at 400 r.p.m., 22 °C in borate-buffered saline, pH 8.2, containing EDTA-free protease inhibitor cocktail, 2.5 mg/mL lysozyme and 40 U/mL benzonase. Fab-containing bacteria lysate was blocked with Superblock and used for ELISA screening, and the reactivity to four different antigens was assessed in parallel. The following antigens were coated on separate

384-well ELISA plates: anti-Fd antibody (The Binding Site) 1:1,000 in PBS, to check the expression level of each Fab clone in bacteria; $rmPrP_{23-231}$ at 87 nM in PBS, to identify candidate PrP^{C} binders; $mPrP^{2cys}$ at 87 nM in PBS, to check for cross reactivity with $mPrP^{2cys}$; neutravidin at 87 nM as a control for specificity. Antigen-coated ELISA plates were washed twice with PBS-T and blocked with Superblock for 2 hours. Fab-containing bacteria lysates from the expression plate were transferred to corresponding wells of the ELISA plates. After 2 hours of incubation, ELISA plates were washed 3 times with PBS-T, and anti-human-F(ab′)2-alkaline-phosphatase-conjugated antibody (1:5,000 in PBS-T) was added. After 1 hour of incubation at room temperature, followed by 3 washings with PBS-T, pNPP substrate was added and, after 5 min incubation, the ELISA signal was measured at 405 nm. Fabs from bacteria lysates producing an ELISA signal 5 times higher than the technical background, which was calculated as the average of the coated well containing un-inoculated medium, and negative for neutravidin were considered as PrP^{C} binder candidates. For hit selection, we considered only anti-PrP^{C} Fabs whose ELISA signal for $rmPrP_{23-231}$ was at least two times higher than for $mPrP^{2cys}$. All the identified hits were checked in a confirmatory ELISA screening. Bacterial cultures of the selected clones were used for DNA minipreps followed by Sanger sequencing using the following sequencing primers: HuCAL_VH (5′-GATAAGCATGCGTAGGAGAAA-3′) and M13Rev (5′-CAGGAAACAGCTATGAC-3′).

Expression and purification of selected anti-PrP Fabs. Chemically competent BL21(D3) cells (Invitrogen) were transformed with selected pPE2-Fab plasmids and grown on plates with LBagar, kanamycin and 1% glucose. A single colony was inoculated into 20 mL of 2×YT, kanamycin and 1% glucose pre-culture medium and incubated for at least 4 hours at 37 °C, 220 r.p.m. One liter of 2YT medium containing kanamycin and 0.1% glucose was inoculated with 20 mL pre-culture, and Fab expression was induced by 0.75 mM IPTG followed by incubation overnight at 25 °C, 180 r.p.m. The overnight culture was centrifuged at 4,000*g* at 4 °C for 30 minutes, and the pellet was frozen at −20 °C. For Fab purification, the thawed pellet was resuspended into 20 mL lysis buffer (0.025 M Tris pH 8; 0.5 M NaCl; 2 mM $MgCl_2$; 100 U/mL benzonase (Merck); 0.25 mg/mL lysozyme (Roche), EDTA-free protease inhibitor (Roche)) and incubated for 1 hour at room temperature at 50 r.p.m. The lysate was centrifuged at 16,000*g* at 4 °C for 30 minutes, and supernatant was filtrated through 0.22-µM Millipore Express Plus Membrane. Fab purification was achieved via the His_6-Tag of the heavy chain by IMAC. Briefly, after equilibration of the Ni-NTA column with running buffer (20 mM Na-phosphate buffer, 500 mM NaCl, 10 mM imidazole, pH 7.4), and the bacteria lysate was loaded and washed with washing buffer (20 mM Na-phosphate buffer, 500 mM NaCl, 20 mM Imidazole, pH 7.4). The Fab was eluted with elution buffer (20 mM Na-phosphate buffer, 500 mM NaCl, 250 mM imidazole, pH 7.4). Buffer exchange was performed using PD-10 columns, Sephadex G-25M (Sigma), whereby the Fab was eluted with PBS.

Förster resonance energy transfer. Europium (Eu^{3+}) donor fluorophore was coupled to POM1 (yielding POM1-Eu^{3+}) and allophycocyanin (APC) acceptor fluorophores was coupled to holoantibody POM3 (yielding holo-POM3-APC) as previously described[26]. Full-length, recombinant mouse prion protein ($rmPrP_{23-231}$) was added at a final concentration of 1.75 nM, followed by addition of holo-POM3-APC at a final concentration of 5 nM and subsequent incubation at 37 °C for 30 minutes with constant shaking at 400 r.p.m. Pomologs were then added in serial dilutions from 0 to 3 nM and were again incubated at 37 °C for 60 minutes with constant shaking at 400 r.p.m., followed by addition of POM1-Eu^{3+} at a final concentration of 2.5 nM). Net Förster resonance energy transfer (FRET) was calculated as described previously[26].

Determination of binding constants from Förster resonance energy transfer. The dependence of the FRET signal on POM1 concentration was modelled by a simple competitive binding model. The binding constant of the FRET-labeled POM1-Eu^{3+} was defined as:

$$K_F = \frac{[PrP_{free}] \times [F_{free}]}{[F_b]} = \frac{([PrP_{tot}] - [F_b] - [A_b]) \times ([F_{tot}] - [F_b])}{[F_b]}$$

where square brackets denote concentration, F_{tot}, F_{free} and F_b denote total, free and bound POM1-Eu^{3+}, PrP_{tot} and PrP_{free} denote the total and free PrP, A_{tot}, A_{free} and A_b denote total, free and bound single-chain fragment variables (scFvs) and K_F is the binding constant of POM1-Eu^{3+}. The righthand equality is obtained by imposing conservation of mass. An equivalent equation defines the binding constant of the scFvs:

$$K_D = \frac{[PrP_{free}] \times [A_{free}]}{[A_b]} = \frac{([PrP_{tot}] - [F_b] - [A_b]) \times ([A_{tot}] - [A_b])}{[A_b]}$$

This system of equations is solved to give F_b as a function of A_{tot}. To relate the concentration of bound POM1-Eu^{3+}, F_b, to the FRET measurements, this equation was rescaled to 100 for the fully bound and 10 for the fully unbound limit. An additional complication in interpreting the experimental data stems from the fact that a FRET signal will appear only if both a POM1-$Eu^{3+}$and holo-POM3-APC are bound to the same PrP. We assume that the binding of POM1 and POM3 is independent, so we can approximate the concentration of PrP bound to a holo-POM3-APC as the effective PrP concentration, PrP_{tot} in the above equations. The binding constant of holo-POM3-APC was determined to be 0.23 nM, giving an effective concentration of PrP of 1.64 nM (compared with the total PrP concentration of 1.75 nM). To verify the robustness of these results, we fitted the data assuming a much weaker binding of holo-POM3-APC, with a binding constant of 1 nM. The obtained K_D values of the single-chain fragments were within the error of the ones determined with a holo-POM3-APC binding constant of 0.23 nM.

Immunohistochemical stainings and analysis of immunofluorescence. COCS were washed twice in PBS and fixed in 4% paraformaldehyde for at least 2 days at 4 °C and were washed again twice in PBS prior to blocking of unspecific binding by incubation in blocking buffer (0.05% Triton X-100 vol/vol, 0.3% goat serum vol/vol in PBS) for 1 hour at room temperature. For visualization of neuronal nuclei, the monoclonal mouse anti-NeuN antibody conjugated to Alexa Fluor 488 (clone A60, Life Technologies) was dissolved at a concentration of 1.6 µg mL^{-1} into blocking buffer and incubated for 3 days at 4 °C. Further primary antibodies used were recombinant anti-calbindin antibody (1 µg mL^{-1}, ab108404, Abcam), anti-glial fibrillary acidic protein (1:500, Z0334, DAKO) and anti-F4/80 (1 µg mL^{-1}, MCAP497G, Serotec). Unconjugated antibodies were dissolved in blocking buffer and incubated for 3 days at 4 °C. After 3 washes with PBS for 30 minutes, COCS were incubated for 3 days at 4 °C with secondary antibodies Alexa-Flour-594-conjugated goat anti-rabbit-IgG (Life Technologies) or Alexa-Fluor-647-conjugated goat anti-rat-IgG (Life Technologies) at a dilution of 1:1,000 in blocking buffer. Slices were then washed with PBS for 15 minutes and incubated in DAPI (1 µg mL^{-1}) in PBS at room temperature for 30 minutes to visualize cell nuclei. Two subsequent washes in PBS were performed, and COCS were mounted with fluorescence mounting medium (DAKO) on glass slides. NeuN, GFAP, F4/80 and calbindin morphometry was performed by image acquisition on a fluorescence microscope (BX-61, Olympus), and analysis was performed using gray-level auto thresholding function in ImageJ (www.fiji.sc). Cell numbers in Figure 2f were determined using the 'Spots' function in Imaris (Oxford Instruments). Morphometric quantification was done on unprocessed images with identical exposure times and image thresholds between compared groups. Representative fluorescent micrographs in the main and supplementary figures have been processed (linear adjustment of brightness and contrast) for better interpretability.

For immunohistochemistry of CAD5 cells, cells were seeded on 18-well µ-slides (Ibidi) and fixed with 4% paraformaldehyde for 5 minutes at room temperature. Unspecific reactions were blocked using 3% goat serum in PBS for 1 hour at room temperature. Mouse monoclonal anti-PrP^{C} antibodies POM1, POM5, POM8 and POM19 (all holo-antibodies) were established before[25]; POM antibodies were incubated at 4 µg mL^{-1} in 3% goat serum in PBS at 4 °C, followed by 3 washes in PBS. Antibodies were detected using Alexa-Fluor-488-conjugated goat anti-mouse-IgG at 1:250 dilution, followed by nuclear counterstain with DAPI (1 µg mL^{-1} in PBS) for 5 minutes at room temperature. Image analysis was performed using SP5 confocal microscope (Leica) with identical exposure times across different experimental groups.

In vitro toxicity assessment. Quantification of POM1 toxicity on CAD5 *Prnp*$^{-/-}$ cells stably transfected with $mPrP^{C}$, $mPrP^{C}_{R207A}$ or empty control vector, as described above, was measured as percentage of PI-positive cells using flow cytometry, as described before[11].

CAD5 cells were cultured with 20 mL Corning Basal Cell Culture Liquid Media–DMEM and Ham's F-12, 50/50 Mix, supplemented with 10% FBS, Gibco MEM Non-Essential Amino Acids Solution 1×, Gibco GlutaMAX Supplement 1× and 0.5 mg/mL of Geneticin in T75 Flasks (Thermo Fisher) at 37 °C, 5% CO_2. Sixteen hours before treatment, cells were split into 96-well plates at 25,000 cells/well in 100 µL.

POM1 alone was prepared at 5 µM final concentration in 20 mM HEPES pH 7.2 and 150 mM NaCl, and 100 µL of each sample, including buffer control, was added to CAD5 cells, in duplicates.

After 48 hours, cells were washed 2 times with 100 µL MACS buffer (PBS + 1% FBS + 2 mM EDTA) and resuspended in 100 µL MACS buffer. Thirty minutes before FACS measurements, PI (1 µg/mL) was added to the cells. Measurements were performed using a BD LSRFortessa. The percentages of PI-positive cells were plotted in columns as mean with s.d. The gating strategy is depicted in Extended Data Figure 3a.

In vivo toxicity assessment. The in vivo toxicity assessment was performed as previously described[9]. In brief, mice where i.c. injected using a motorized stereotaxic frame (Neurostar) at the following bregma coordinates (AP −2 mm, ML ±1.7 mm, DV 2.2mm, angle in ML/DV plane 15°). Antibodies (2 µL) were injected at a flow rate of 0.5 µL/minute. After termination of the injection, the needle was left in place for 3 minutes.

Twenty-four hours after stereotactic injection, mice were placed on a bed equipped with a mouse whole-body radio frequency transmitter coil and a mouse head surface-coil receiver and then transferred into the 4.7 Bruker Pharma scan. For DWI, routine gradient echo sequences with the following parameters were

used: TR: 300 ms TE: 28 ms, flip angle: 90°, average: 1, matrix: 350 × 350, field of view: 3 × 3 cm, acquisition time: 17 minutes, voxel size: 87 × 87 μm^3, slice thickness: 700 µm, isodistance: 1,400 μm^3 and *b* values: 13,816 s/mm^2. Finally, mice were euthanized after 49 hours, and the brains were fixed in 4% formalin. Coronal sections from the posterior cortex were paraffin-embedded (4 mm) and 2-µm coronal step sections (standard every 100 µm) were cut, deparaffinized and routinely stained with hematoxylin and eosin.

Dose–response analysis and the benchmark dose relation were calculated with benchmark dose software (BMDS) 2.4 (United States Environmental Protection Agency).

Molecular dynamics. Experimental structures were used as a basis for MD simulations when available (scPOM1–mPrP complex, Protein Data Bank (PDB) 4H88; free mPrP, PDB 1XYX). The structures of full-length mPrP, $mPrP_{\Delta 90-231}$ and the pomologs were predicted by homology modeling on the I-Tasser webserver[27], on the basis of the experimental structure of the PrP globular domain (aa 120–231), and were further validated with MD.

In all simulations, the system was initially set up and equilibrated through standard MD protocols: proteins were centered in a triclinic box, 0.2 nm from the edge, and filled with SPCE water model and 0.15 M Na^+Cl^- ions using the AMBER99SB-ILDN protein force field; energy minimization followed. Temperature (298 K) and pressure (1 bar) equilibration steps (100 ps each) were performed. Three independent replicates of 500-ns MD simulations were run with the above-mentioned force field for each protein or complex. MD trajectory files were analyzed after removal of periodic boundary conditions. The overall stability of each simulated complex was verified by root mean square deviation, radius of gyration and visual analysis, according to standard procedures. Structural clusters, atomic interactions and root mean square fluctuation (RMSF) were analyzed using GROMACS[28] and standard structural biology tools. RMSF provides a qualitative indication of residue level flexibility, as shown in Figure 1c.

The presence of H-bonds or other interactions between GD residues was initially estimated by visual analysis and then by distance between appropriate chemical groups during the simulation time.

Nuclear magnetic resonance. Spectra were recorded on a Bruker Avance 600 MHz NMR spectrometer at 298 K, pH 7 in 50 mM sodium phosphate buffer at a concentration of 300 µM. In mapping experiments, mPrP was uniformly labeled with ^{15}N (99%) and ^{2}H (approx. 70%); antibodies were unlabeled. PrP and antibody samples were freshly prepared and extensively dialyzed against the same buffer prior to complex formation. The same procedure was followed for CD measurements. Chemical-shift assignment was based on published data (Biological Magnetic Resonance Data Bank entry 16071)[29]. Briefly, overlay of [^{15}N,^{1}H]-TROSY spectra of free or bound $mPrP_{90-231}$ allowed for identification of PrP residues for which the associated NMR signal changed upon complex formation, indicating alterations in their local chemical environment[19].

Phage display. A synthetic human Fab phagemid library (Novartis Institutes for BioMedical Research) was used for phage display. First, two rounds of selection against PrP^C were performed by coating 96-well Maxisorp plates (Nunc) with a decreasing amount of $rmPrP_{23-231}$ (1 µM and 0.5 µM respectively, in PBS), overnight at 4 °C. PrP-coated plates were washed 3 times with PBS-T and blocked with Superblock for 2 hours. Input of 4×10^{11} phages in 300 µL PBS was used for the first round of panning. After 2 hours of blocking with Chemiblocker (Millipore), the phages were incubated with PrP-coated wells for 2 hours at room temperature. The non-binding phages were then removed by extensive washing with PBS-T, while $rmPrP_{23-231}$-bound phages were eluted with 0.1 M glycine/HCl, pH 2.0 for 10 minutes at room temperature; the pH was then neutralized by 1 M Tris pH 8.0. Eluted phages were used to infect exponentially growing amber suppressor TG1 cells (Lubio Science). Infected bacteria were cultured in 2YT, carbenicillin and 1% glucose medium overnight at 37 °C, 200 r.p.m., and superinfected with VCSM13 helper phages. The production of phage particles was then induced by culturing the superinfected bacteria in 2YT, carbenicillin and kanamycin medium containing 0.25 mM isopropyl β-D-1-thiogalactopyranoside (IPTG), overnight at 22 °C, 180 r.p.m. Supernatant containing phages from the overnight culture was used for the second panning round. Output phages from the second round were purified by PEG/NaCl precipitation, titrated and used in the following third rounds to enrich phage-displayed Fabs that bound preferentially $mPrP^C$ over $mPrP^{2cys}$.

Two strategies were used: depletion of binders to recombinant $mPrP^{2cys}$ by subtraction in solid phase and depletion of $mPrP^{2cys}$ binders by competition with $rhPrP^C_{23-230}$-AviTag in liquid phase. In the former setting, purified phages were first exposed to 0.75 µM $mPrP^{2cys}$ (threefold molar excess compared with $rmPrP_{90-231}$ or $rmPrP_{121-231}$), and then the unbound phages were selected for $rmPrP_{90-231}$ or $rmPrP_{121-231}$ binders. Alternatively, purified phages were first adsorbed on neutravidin-coated wells to remove the neutravidin binders and then exposed to 0.25 µM $rhPrP^C_{23-230}$-AviTag in solution in the presence of 0.75 µM (threefold molar excess) of $mPrP^{2cys}$. The phage-displayed Fabs binding to $rhPrP^C_{23-230}$-AviTag were captured on neutravidin-coated wells and eluted as described above. For both strategies, a fourth panning round was performed using 0.3 µM $mPrP^{2cys}$ for depletion and 0.1 µM $rmPrP_{121-231}$ (coated on the plate) or $rhPrP^C_{23-230}$-AviTag (in solution) for positive selection. At the fourth round of selection, DNA minipreps were prepared from the panning output pools by QIAprep Spin Miniprep kit (Qiagen) and the whole anti-PrP Fab enriched library was subcloned in expression vector pPE2 (kindly provided by Novartis). DNA was then used to transform electrocompetent non-amber suppressor MC1061 bacteria (Lubio Science) to produce soluble Fabs and perform ELISA screening.

Production of recombinant proteins and antibodies. Bacterial production of recombinant, full-length mouse PrP_{23-231}, recombinant fragments of human and mouse PrP and recombinant, biotinylated human PrP^C-AviTag ($rhPrP^C_{23-230}$-AviTag) was achieved as previously described[30–32]. Production of scFv and the IgG POM1 antibodies used in this manuscript was performed as described before[25]. Production of holo-^{hc}Y104A was performed as follows: POM1 IgG_1 heavy chain containing a Y104A mutation and POM1 kappa light chain were ordered as a bicistronic synthetic DNA block (gBlock, IDT) separated by a P2A site. The synthetic gene block (gBlock, IDT, see full sequence in the Supplementary Information) was then cloned into pcDNA 3.4-TOPO vector (Thermo Fisher Scientific), and recombinant expression was achieved using the FreeStyle MAX 293 Expression System (Thermo Fisher Scientific), according to the manufacturer's guidelines. Glucose levels were kept constant over 25 mM. Seven days after cell transfection, medium supernatant was collected, centrifuged and filtered. A Protein-G column (GE Healthcare) was used for affinity purification of antibodies, followed by elution with glycine buffer (pH 2.6) and subsequent dialysis against PBS (pH 7.2–7.4). Purity was determined by SDS–PAGE, and protein concentrations were determined using Pierce BCA Protein Assay Kit (Thermo Fisher Scientific). For generation of POM1 mutants, we performed site-directed mutagenesis on a POM1 pET-22b(+) (Novagen) expression plasmid[7] according to the manufacturer's guidelines (primers (5′→3′): ^{hc}W33A: forward (FW): CATTCA CTGACTACGCGATGCACTGGGTGAAGC, reverse (REV): GCTTCACCCAG TGCATCGCGTAGTCAGTGAATG. ^{hc}D52A: FW: GAGTGGATCGGATCGATT GCGCCTTCTGATAG, REV: CTATCAGAAGGCGCAATCGATCCGATCCACTC. ^{hc}D55A: FW GGATCGATTGATCCTTCTGCGAGTTATACTAGTCAC, REVGT GACTAGTATAACTCGCAGAAGGATCAATCGATCC. ^{hc}Y57A: FW: CCTTCTGA TAGTGCGACTAGTCACAATGAAAAGTTCAAGG, REV: CCTTGAACTTTTC ATTGTGACTAGTCGCACTATCAGAAGG. ^{lc}S32A: FW: CCAGTCAGAACATT GGCACAGCGATACACTGGTATCAGCAAAG, REV: CTTTGCTGATACCAG TGTATCGCTGTGCCAATGTTCTGACTGG. ^{lc}Y50A: FW: CTCCAAGGCTTAT CATAAAGGCGGCTTCTGAGTCTATCTCTGG, REV: CCAGAGATAGACTCAG AAGCCGCCTTTATGATAAGCCTTGGAG. ^{lc}S91A: FW: CAGATTATTACTGTC AACAAGCTAATACCTGGCCGTACACGTT, REV: AACGTGTACGGCCAGG TATTAGCTTGTTGACAGTAATAATCTG. ^{lc}W94A: FW: GTCAACAAAGTAATA CCGCGCCGTACACGTTCGGAGG, REV: CCTCCGAACGTGTACGGCGCGG TATTACTTTGTTGAC. ^{lc}Y96A: FW: TAATACCTGGCCGGCCACGTTCGGA GGGG, REV: CCCCTCCGAACGTGGCCGGCCAGGTATTA. ^{hc}Y101A: FW: CTGTTCAAGATCCGGCGCCGGATATTATGCTATGGAG, REV: CTCCATAG CATAATATCCGGCGCCGGATCTTGAACAG. ^{hc}Y104A: FW: CCGGCTACGGA TATGCTGCTATGGAGTACTGGG, REV: CCCAGTACTCCATAGCAGCATA TCCGTAGCCGG), followed by subsequent expression and purification as was described for holo-POM1.

Protein analysis. COCS were washed twice in PBS and scraped off the PTFE membranes with PBS. Homogenization was performed with a TissueLyser LT (Qiagen) for 2 minutes at 50 Hz. A bicinchoninic acid assay (Pierce BCA Protein Assay Kit, Thermo Fisher Scientific) was used to determine protein concentrations. PrP^{Sc} levels were determined through digestion of 20 µg of COCS homogenates with 25 µg mL^{-1} of proteinase K (PK, Roche) at a final volume of 20 µL in PBS for 30 minutes at 37 °C. PK was deactivated by addition of sodium-dodecyl-sulfate-containing NuPAGE LDS sample buffer (Thermo Fisher Scientific) and boiling of samples at 95 °C for 5 minutes. Equal sample volumes were loaded on Nu-PAGE Bis/Tris precast gels (Life Technologies) and PrP^C/PrP^{Sc} was detected by western blot using the monoclonal anti-PrP antibodies POM1, POM2 or POM19 at 0.4 µg mL^{-1} (all holo-antibodies), as established elsewhere[8]. Further primary antibodies used for western blots in this manuscript are as follows: monomeric NeonGreen (1:1,000, 32F6, Chromotek), phospho-eIF2α (1:1,000, clone no. D9G8, Cell Signaling Technologies), eIF2α (1:1,000, clone no. D7D3, Cell Signaling Technologies), pan-actin (1:10,000, clone no. C4, Millipore), GFAP (1:1,000, clone no. D1F4Q, Cell Signaling Technologies), Iba1 (1:500, catalog no. 019–19741, Wako), NeuN (0.5 µg/ml, catalog no. ABN78, Merck Millipore) and Myc-tag (1:500, catalog no. ab9106, Abcam). After incubation of primary antibodies at 4 °C overnight, membranes were washed and detected with goat polyclonal anti-mouse (1:10,000, 115–035–062, Jackson ImmunoResearch) or goat polyclonal anti-rabbit (1:10,000, 111–035–045, Jackson ImmunoResearch) antibodies for 1 hour at room temperature. For PNGaseF digestion, 20 µg of samples was processed using a commercially available kit (New England Biolabs), and PrP^C detection was performed using the monoclonal anti-PrP^C antibody POM2, as described above. Western blots were quantified on native photographs (uncropped, naive images are available in the Source Data); representative western blot images in the main and supplementary figures have been processed (linear adjustment of contrast and brightness) for better visualization.

Surface plasmon resonance (SPR). The binding properties of the complexes between rmPrP, POM1 and pomologs were measured at 298 K on a ProteOn XPR-36 instrument (Bio-Rad) using 20 mM HEPES pH 7.2, 150 mM NaCl, 3 mM EDTA and 0.005% Tween-20 as running buffer. mPrP was immobilized on the surface of GLC sensor chips through standard amide coupling. Serial dilution of antibodies (full IgG, Fab or single-chain versions) in the nanomolar range were injected at a flow rate of 100 µL/min (contact time 6 minutes); the dissociation phase was then observed for 5 minutes. Analyte responses were corrected for unspecific binding and buffer responses by subtracting the signal of both a channel where no PrP was immobilized and a channel with no antibody was added. Curve fitting and data analysis were performed with Bio-Rad ProteOn Manager software (version 3.1.0.6).

Statistical analyses. All biological measurements are taken from distinct samples. Unless mentioned otherwise, the following tests were performed for statistical hypothesis testing: unpaired, two-tailed *t*-test was used for comparison between two groups, one-way ANOVA with Dunnett's multiple-comparison test was used for comparison of multiple groups with a control group, and ordinary one-way ANOVA with Šídák's multiple comparisons test was used for comparison of preselected pairs of groups. Statistical analysis and visualization were performed using Prism 8 (GraphPad). No statistical methods were used to pre-determine sample sizes, but our sample sizes are similar to those reported in previous publications[7–11]. Except for in vivo prion inoculation experiments and NeuN morphometry, data collection and analysis were not performed blind to the conditions of the experiments.

Synchrotron radiation circular dichroism. Secondary structure content of complexes between rmPrP and POM1 and ^{hc}Y57 and ^{hc}Y104A was analyzed with synchrotron radiation circular dichroism (SRCD) spectroscopy.

Experiments were performed using a nitrogen-flushed B23 beamline for SRCD at Diamond Light Source or ChirascanPlus CD spectropolarimeter (Applied Photophysics). With both instruments, scans were acquired at 20 °C using an integration time of 1 second and 1 nm bandwidth. Demountable cuvette cells with a pathlength of 0.00335 cm were used in the far-UV region (180–260 nm) to measure the CD of the protein concentration, varying from 10 to 102 µM protein in 10 mM NaP pH 7 and 150 mM NaCl. Mixtures were prepared to a stoichiometric molar ratio of 1:1. SRCD data were processed using CDApps[33] and OriginLab. Spectra have been normalized using an average amino acid molecular weight of 113 for secondary structure estimation from SRCD, and CD spectra were created using CDApps using the Continll algorithm[34]. For comparison of calculated and observed spectra, the full molecular weight of sample and complex were used. Measurements of free mPrP and free antibodies were taken as a reference.

Reporting summary. Further information on research design is available in the Nature Research Reporting Summary linked to this article.

Data availability

All source data, for example numeric source data, uncropped western blot gels including annotations thereof, as well as unique DNA sequences, accompany this manuscript as supplements. The following publicly available data was used: Allen Mouse Brain Atlas, entries 71717640 and 227540 (https://mouse.brain-map.org); Biological Magnetic Resonance Data Bank, entry 16071 (https://bmrb.io/); RCSB Protein Data Bank, entries 1XYX and 4H88 (https://www.rcsb.org). Additionally, all unique biological materials used in the manuscript are readily available from the authors. Source data are provided with this paper.

Code availability

New code was generated for analysis of Allen Brain Atlas data and can be found in the Supplementary Software.

References

23. Rincon, M. Y. et al. Widespread transduction of astrocytes and neurons in the mouse central nervous system after systemic delivery of a self-complementary AAV-PHP.B vector. *Gene Ther.* **25**, 83–92 (2018).
24. Herrmann, U. S. et al. Structure-based drug design identifies polythiophenes as antiprion compounds. *Sci. Transl. Med.* **7**, 299ra123 (2015).
25. Polymenidou, M. et al. The POM monoclonals: a comprehensive set of antibodies to non-overlapping prion protein epitopes. *PLoS One* **3**, e3872 (2008).
26. Ballmer, B. A. et al. Modifiers of prion protein biogenesis and recycling identified by a highly parallel endocytosis kinetics assay. *J. Biol. Chem.* **292**, 8356–8368 (2017).
27. Yang, J. et al. The I-TASSER Suite: protein structure and function prediction. *Nat. Methods* **12**, 7–8 (2015).
28. Berendsen, H. J. C., van der Spoel, D. & van Drunen, R. GROMACS: a message-passing parallel molecular dynamics implementation. *Comput. Phys. Commun.* **91**, 43–56 (1995).
29. Hornemann, S., von Schroetter, C., Damberger, F. F. & Wuthrich, K. Prion protein-detergent micelle interactions studied by NMR in solution. *J. Biol. Chem.* **284**, 22713–22721 (2009).
30. Hornemann, S., Christen, B., von Schroetter, C., Perez, D. R. & Wuthrich, K. Prion protein library of recombinant constructs for structural biology. *FEBS J.* **276**, 2359–2367 (2009).
31. Zahn, R., von Schroetter, C. & Wuthrich, K. Human prion proteins expressed in *Escherichia coli* and purified by high-affinity column refolding. *FEBS Lett.* **417**, 400–404 (1997).
32. Frontzek, K. et al. Autoantibodies against the prion protein in individuals with PRNP mutations. *Neurology* **2020**, 1–10 (2020).
33. Hussain, R. et al. CDApps: integrated software for experimental planning and data processing at beamline B23, Diamond Light Source. Corrigendum. *J. Synchrotron Radiat.* **22**, 862 (2015).
34. Provencher, S. W. & Glockner, J. Estimation of globular protein secondary structure from circular dichroism. *Biochemistry* **20**, 33–37 (1981).

Acknowledgements

We would like to acknowledge M. Epskamp, T. Kottarathil, M. Carta, M. Rincon, R. Moos, J. Guo and C. Tournaire for valuable discussions and technical help, as well as T. Sonati for advising on certain experiments performed by C. Tournaire. We are grateful to G. Moro for help and discussion. Imaging was performed with equipment maintained by the Center of Microscopy and Image Analysis, University of Zurich. The viral vectors and respective plasmids were produced by the Viral Vector Facility (VVF) at the Neuroscience Center Zurich (Zentrum für Neurowissenschaften Zürich, ZNZ). We are grateful to A. P. Valente for useful discussion on protein dynamics. K. F. received unrestricted support from the Theodor und Ida Herzog-Egli-Stiftung and Ono Pharmaceuticals. R. R. R. was supported by a Career Development Award from the Stavros Niarchos Foundation. G. M. is funded by a Ramon Jenkins Research Fellowship at Sidney Sussex College. T. K. received financial support from the EPSRC, BBSRC, ERC, and the Frances and Augustus Newman Foundation. A. A. is supported by an Advanced Grant of the European Research Council (ERC, No. 250356), a Distinguished Scientist Award from the Nomis Foundation and grants from the GELU Foundation, the Swiss National Science Foundation (SNSF grant ID 179040, including a Sinergia grant), and the Swiss Initiative in Systems Biology, SystemsX.ch (PrionX, SynucleiX). L. V. gratefully acknowledges support from SNF (nos. 310030_166445, 157699), Synapsis Foundation_Alzheimer research (ARS) and Lions Club Monteceneri. We would like to thank Diamond Light Source for B23 beamtime allocation (CM-19680). M. G. H. was supported by a grant from the Thierry Latran Foundation (SOD-VIP), The Research Foundation – Flanders (FWO, grant 1513616N), European Research Council (ERC) Proof of Concept Grant 713755 – AD-VIP) and the European Commission (H2020-WIDESPREAD-2018–2020–6; NCBio; 951923).

Author contributions

A. A. and L. V. conceived and supervised the project, acquired funds and provided experimental resources. K. F. conceptualized, performed and analyzed slice culture experiments (except those depicted in Figure 7) and in vitro and AAV therapy experiments. M. B. cloned, produced and characterized all scFv antibodies used in this manuscript. NMR experiments were performed by M. B., L. S., S. J. and O. Z.. M. B. conceptualized, performed and analyzed MDS and SPR experiments with support from M. P., F. M. and L. S.. A. S. conceptualized, performed and analyzed all experiments related to phage-display technology and, together with A. H., cloned and performed pilot AAV pomolog experiments. R. R. R. conceptualized, performed and analyzed all MEMRI experiments. S. B. performed and analyzed experiments depicted in Figures 2d and 6h–j under the supervision of K. F. CD Synchrotron experiments were conceptualized, performed and analyzed by R. H. and G. S. M. M. and M. G. H. conceived and produced in vivo AAV pomolog therapies. S. H. and C. Z. supervised and conceptualized experiments carried out by K. F.. P. S. performed in vivo prion inoculations, AAV transductions and necropsies. M. L. designed and cloned non-therapeutic AAV and performed slice culture experiments under the supervision of K. F.. G. M. and T. K. conceptualized and analyzed FRET pomolog binding data. A. L. conceptualized, performed and analyzed in vitro vacuolation experiments. K. F., M. B., M. P., L. S., L. V. and A. A. wrote the original and revised manuscript. All authors performed critical review of both the original and revised version of the manuscript.

Competing interests

The authors declare no competing interests. The funders had no role in study design, data collection and analysis, decision to publish or preparation of the manuscript.

Additional information

Extended data is available for this paper at https://doi.org/10.1038/s41594-022-00814-7.

Supplementary information The online version contains supplementary material available at https://doi.org/10.1038/s41594-022-00814-7.

Correspondence and requests for materials should be addressed to Luca Varani or Adriano Aguzzi.

Peer review information *Nature Structural and Molecular Biology* thanks Jesús Requena and Neil Cashman for their contribution to the peer review of this work. Primary Handling editor: Florian Ullrich, in collaboration with the Nature Structural & Molecular Biology team. Peer reviewer reports are available.

Reprints and permissions information is available at www.nature.com/reprints.

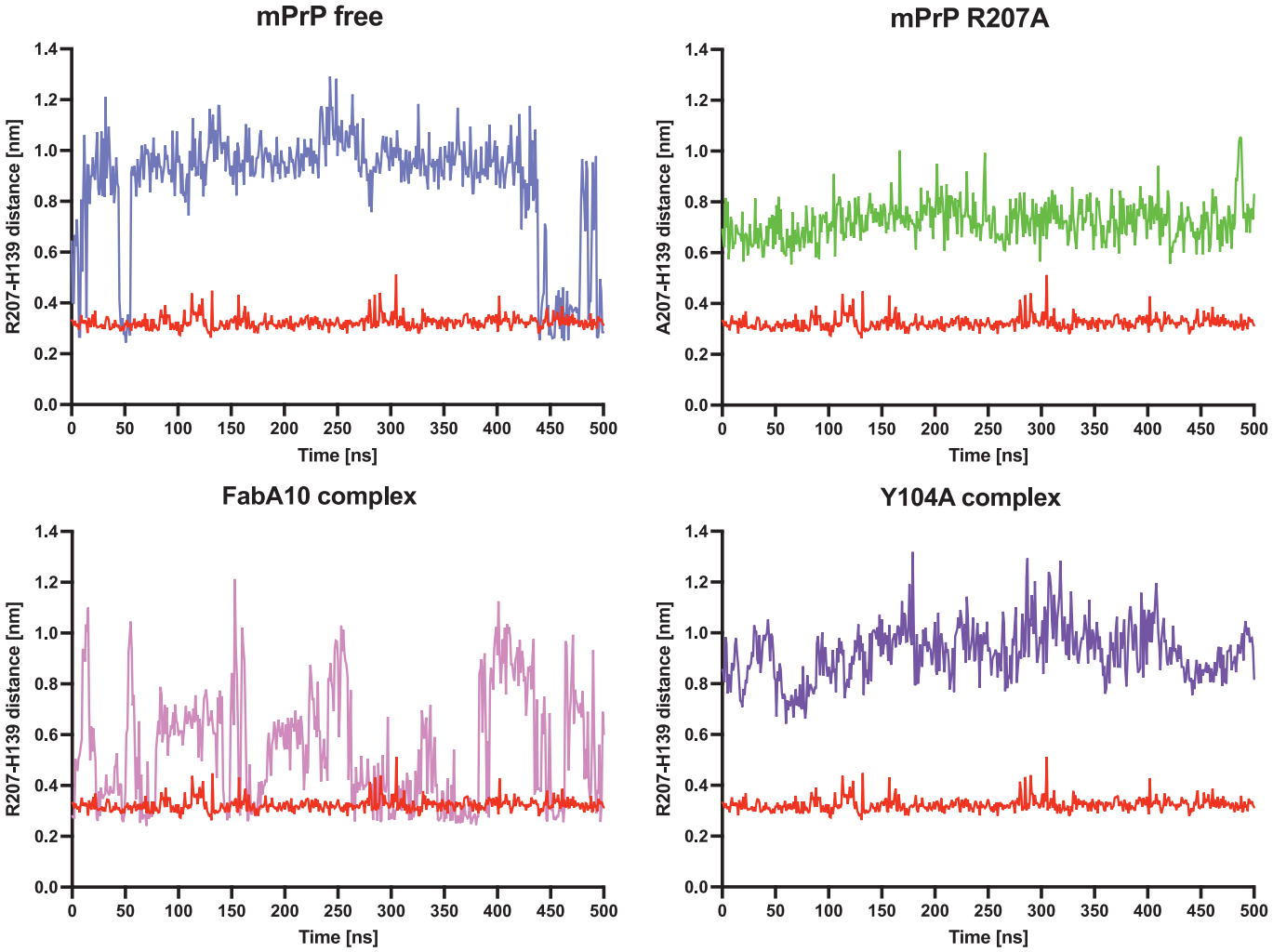

Extended Data Fig. 1 | Distances between the R207 and H139 residues in MD simulations of PrP-antibody complexes. The simulation of the PrP-POM1 complex (red) in reproduced in all charts to facilitate comparisons. When PrP is bound to POM1, the H-bond between R207 and H139 (termed H-latch) is always present, with distance between the centroid of their sidechains around 0.3 nm. Greater distances indicate loss of hydrogen interactions and consequently absence of the H-latch. The complex of PrP with the ^{hc}Y104A pomolog never shows formation of the H-latch, whereas FabA10 shows intermediate values. Simulations were run three times, but only representative traces are shown; aggregated analyses are shown in Fig. 1c.

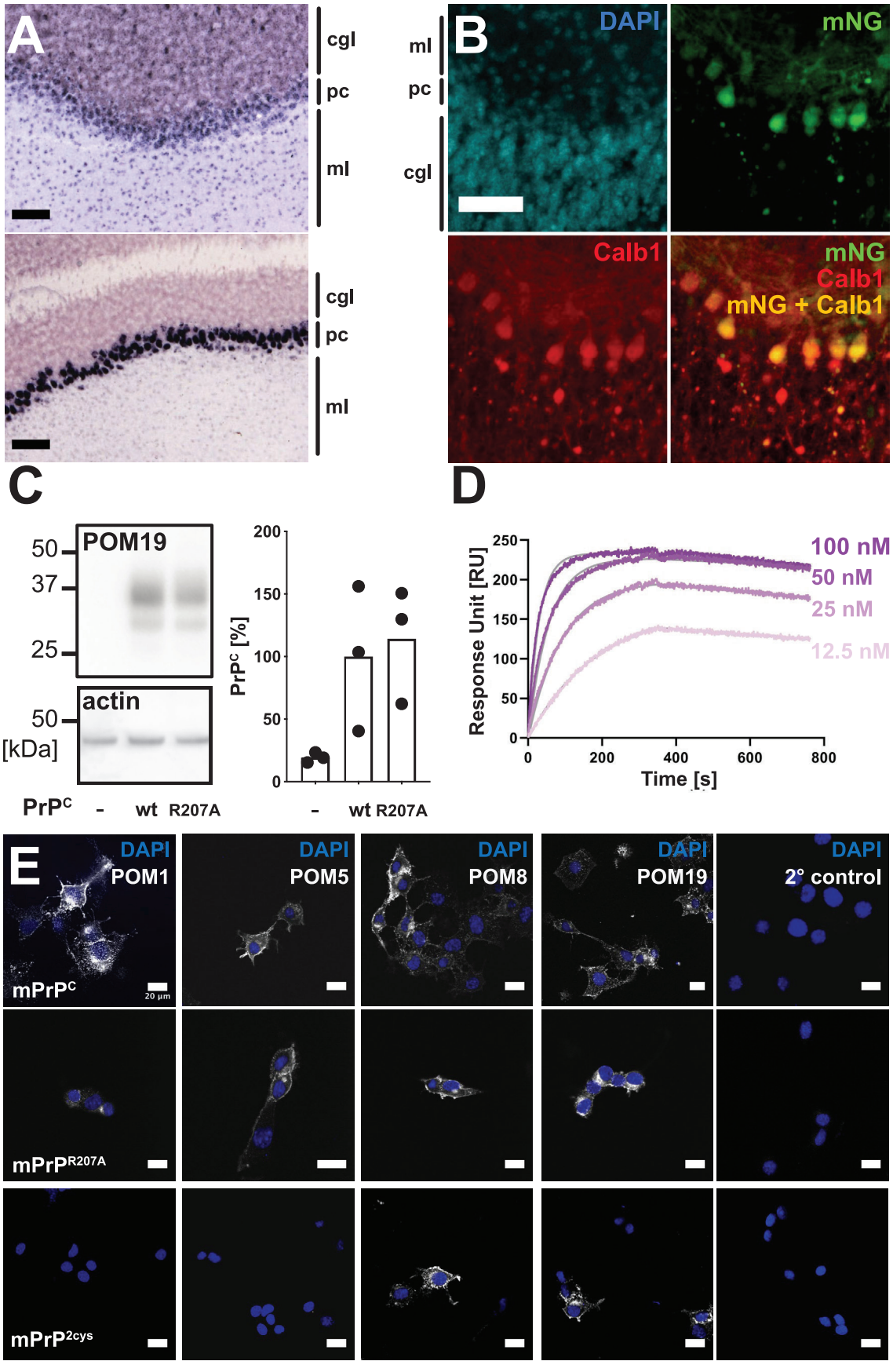

Extended Data Fig. 2 | See next page for caption.

Extended Data Fig. 2 | Robust expression and conformation of the PrPR207A point mutant. (a) Representative images of expression levels of Synapsin 1 (Syn1, *upper*) and Calbindin 1 (Calb1, *lower*) show predominant (Syn1) or almost exclusive (Calb1) expression in Purkinje cells (pc) in the cerebellar cortex. Image credit: Allen Institute. Scale bar = 100 µm. **(b)** Fluorescent micrographs of *Prnp*$^{ZH3/ZH3}$ COCS transduced with the AAV outlined in panel (A) show mNeonGreen expression predominantly in calbindin 1-expressing Purkinje cells. Scale bar = 50 µm. cgl = cerebellar internal granular layer, pc = Purkinje cell layer, ml = molecular layer. These findings were repeated in three independent experiments. **(c)** *Left panel*: Stably transfected CAD5-mPrP^{C} and CAD5-mPrP^{R207A} cells show similar PrP^{C} expression levels. epresentative PrP^{C} levels of one cell culture passage are shown. *Right panel*: POM19 immunoreactivity is divided by actin immunoreactivity, values are given as percentages of PrP^{C}. One datapoint corresponds to one passage of CAD5 cells. **(d)** Surface plasmon resonance (SPR) traces showing binding of POM1 to recombinant mPrP^{R207A} (rmPrP^{R207A}, k_a=3.8E^{+05} 1/Ms, k_d=1.8E^{-04} 1/s, K_D=4.7E^{-10} M; for comparison binding to recombinant wild-type murine PrP showed k_a=3.6E^{+05} 1/Ms; k_d=9.1E^{-05} 1/s; K_D=2.5E^{-10} M). **(e)** Immunohistochemistry of CAD5 *Prnp*$^{-/-}$ cells stably transfected with pcDNA3.1 vector expressing wild-type murine PrP^{C} (mPrP^{C}), mPrP^{R207A} and mPrP^{2cys}. Monoclonal anti-PrP^{C} antibodies targeting distinct conformational epitopes on the globular domain of PrP^{C} were incubated to assess conformational changes in mPrP^{R207A} (POM1: α1-α3, POM5: β2-α2, POM8: α1-α2, POM19: β1-α3). Except for diminished staining of POM1 in mPrP^{R207A}, we observed robust detection of mPrP^{R207A} by POM5, POM8 and POM19 and mPrP^{2cys} by POM8 and POM19. Parts of this experiment, for example POM1 and POM19, were repeated twice. Scale bar = 20 µm.

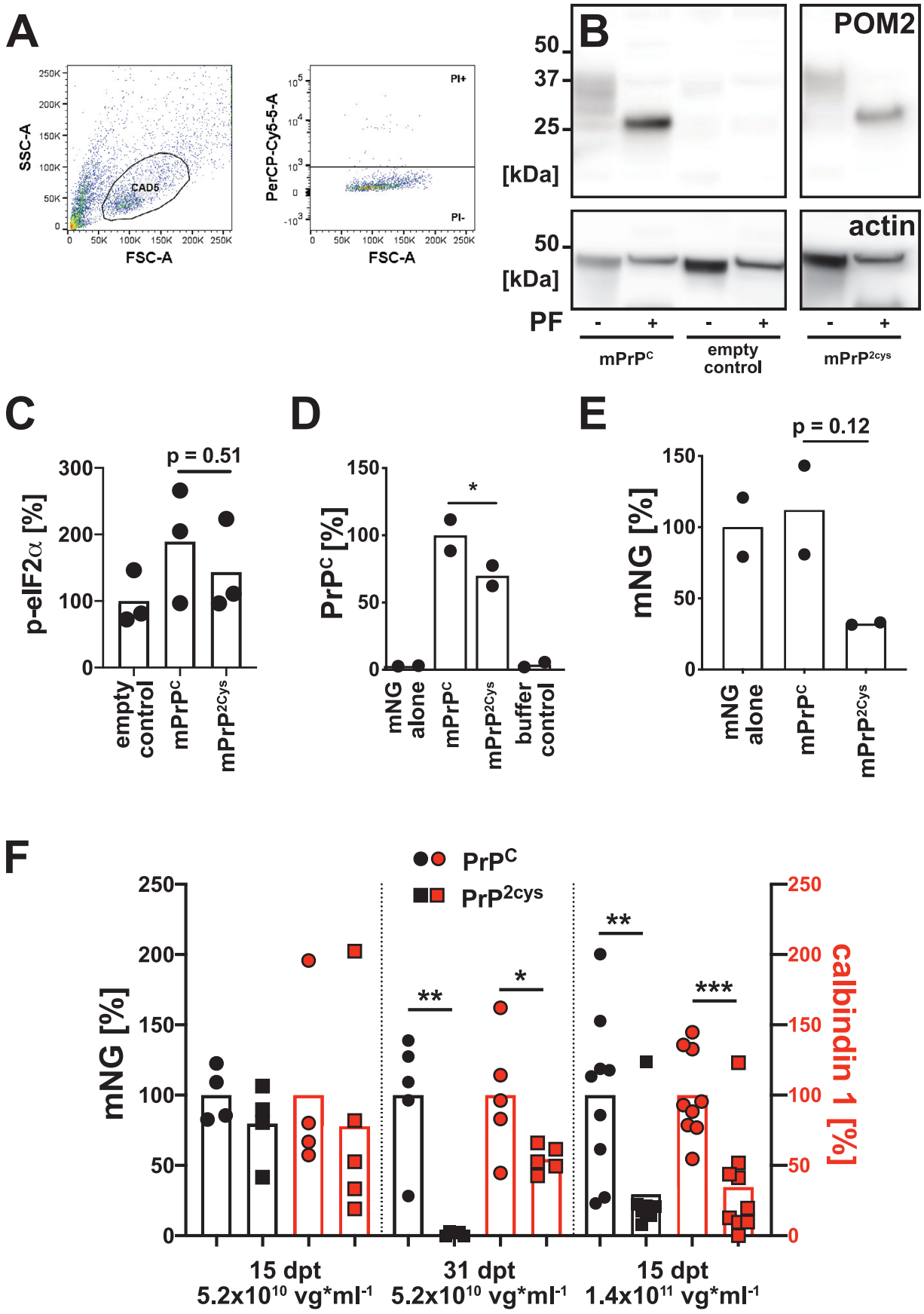

Extended Data Fig. 3 | See next page for caption.